Nuclear Science and Techniques (2026) 37:120
https://doi.org/10.1007/s41365-026-01935-0

Reliability evaluation on partial photoneutron cross sections for $^{142-146,148,150}$Nd

Yu-Long Shen[1,2,3] · Zhi-Cai Li[1,3] · Ting-Kai Ma[1] · Wen-Yu Tan[1] · Ting Wu[1] · Xin-Xiang Li[1,3] · Ji-Min Wang[4] · Xi Tao[4] · Gong-Tao Fan[2] · Rui-Rui Xu[4] · Wen Luo[1,3]

Received: 2 July 2025 / Revised: 21 September 2025 / Accepted: 22 September 2025 / Published online: 11 April 2026

Abstract

Systematic disagreements exist mainly in the available partial photoneutron cross sections $\sigma(\gamma, i\mathrm{nX})$ (i=1, 2), which were measured using quasimonoenergetic annihilation photons at the Saclay (France) and Livermore (USA) laboratories based on neutron multiplicity sorting methods. In this study, the reliability of the $\sigma(\gamma, i\mathrm{nX})$ for $^{142-146,148,150}$Nd isotopes obtained at Saclay was evaluated using an experimental–theoretical method that satisfies the data reliability criteria proposed based on the theoretical model in TALYS. Our evaluations were then compared with the major Evaluated Nuclear Data Libraries, and the differences from the available experimental data were analyzed. It was found that the $\sigma(\gamma, 1\mathrm{nX})$ data of Saclay were overestimated and the $\sigma(\gamma, 2\mathrm{nX})$ data were underestimated in the $^{144-146,148,150}$Nd cases, which is consistent with the conclusion of Varlamov; on the contrary, the $\sigma(\gamma, 1\mathrm{nX})$ were underestimated and the $\sigma(\gamma, 2\mathrm{nX})$ were overestimated in the ^{142,143}Nd cases. Possible reasons for the above inconsistency in the Nd isotopes were further analyzed. Interestingly, subtracting the contribution of isotopic target impurities significantly reduced the discrepancy in the ^{143}Nd case. However, this is no longer applicable to the ^{142}Nd case, and other factors, including the detector efficiency and accidental coincidence events, should be fully considered to resolve such discrepancies.

Keywords Partial photoneutron cross sections · $^{142-146,148,150}$Nd · TALYS · Experimental–theoretical method · Evaluated data

This work was supported by the National Key Research and Development Program (Nos. 2022YFA1603300 and 2022YFA1602403), the National Natural Science Foundation of China (No. 12575133), the Key Laboratory of Nuclear Data Open Fund Project (No. JCKY24201C151), and the Natural Science Foundation of Hunan Province, China (No. 2025JJ60020).

✉ Xin-Xiang Li
lixinxiang@usc.edu.cn

✉ Rui-Rui Xu
xuruirui@ciae.ac.cn

✉ Wen Luo
wenluo-ok@163.com

1 School of Nuclear Science and Technology, University of South China, Hengyang 421001, China

2 Shanghai Advanced Research Institute, Chinese Academy of Sciences, Shanghai 201210, China

3 Key Laboratory of Advanced Nuclear Energy Design and Safety, Ministry of Education, Hengyang 421001, China

4 China Nuclear Data Center, China Institute of Atomic Energy, Beijing 102413, China

1 Introduction

The giant dipole resonance (GDR) [1] is a fundamental collective excitation mode in the nucleus. Measurements of the cross sections of partial photoneutron reactions within the GDR energy range, primarily $(\gamma, 1\mathrm{nX})$ and $(\gamma, 2\mathrm{nX})$, are presented. These data play an important role in obtaining experimental nuclear reaction data. These data are essential for studies on GDR excitation and the competition among its decay channels. In addition, they can be widely used in various applications, including beam luminosity monitoring in ultra-relativistic heavy-ion colliders, non-destructive assay of special nuclear materials, and the development of new production routes for medical radioisotopes [2–5]. Recently, experimental measurements of the photoneutron cross sections for some nuclides of interest, including ^{197}Au, ^{159}Tb, and ^{63}Cu, have been performed and researched at the Shanghai Laser Electron Gamma Source (SLEGS) [6–9]. Neodymium (Nd) isotopes ($^{142-146,148,150}$Nd) are key nuclei for probing the nuclear structure of the giant dipole resonance (GDR) and are important fission products in activation analysis and reactor physics. In 1971, Carlos et al. [10] employed quasimonoenergetic annihilation photon beams [11, 12] based on positron annihilation and a large Gd liquid scintillation detector to measure the photoneutron cross sections for Nd isotopes at the Center d'Etudes Nucleaires of Saclay laboratory (France) [13–15]. The experimental data were included in the experimental nuclear reaction database (EXFOR) [16]. The cross sections for the partial reactions $(\gamma, 1\mathrm{nX})$ and $(\gamma, 2\mathrm{nX})$ of $^{142-146,148,150}$Nd were measured only once using the neutron multiplicity sorting method with a quasimonoenergetic γ-ray source. However, according to Varlamov's research, there may be systematic disagreements in the experimental data based on the Center d'Etudes Nucleaires of Saclay laboratory. An empirical conclusion was proposed and validated for 52 nuclei, excluding Nd. For the experimental data from the Saclay laboratory, the $\sigma(\gamma, 1\mathrm{nX})$ data were overestimated, and the $\sigma(\gamma, 2\mathrm{nX})$ data were underestimated [17–19].

Subsequently, Xu et al. [20] performed preliminary calculations and data evaluations for Nd isotopes using the MEND-G codes [21] in combination with experimental data, and the results were incorporated into CENDL−3.2. However, significant discrepancies exist between the experimental data and the major nuclear data libraries CENDL-Beta [22], IAEA-2019 [23], TENDL-2023 [24], and JENDL-5 [25]. Since experimental measurements serve as a crucial foundation for the photonuclear database, it is worthwhile to evaluate and analyze the reliability of photonuclear data for $^{142-146,148,150}$Nd, thereby supporting systematic evaluations and the development of comprehensive nuclear data libraries.

For data evaluation, γ strength function [26, 27] is important for photoneutron reactions, as it provides the energy-dependent transition strength of γ-rays and is directly related to the spectrum of absorbed γ-rays.

In this study, we evaluated the reliability of the experimental data, analyzed the potential uncertainty in previous experiments, and obtained new evaluated data for Nd isotopes. Including the influence of γ strength function, the optimal model was selected based on its consistency with the experimental cross sections. For the evaluation of $^{144-146,148,150}$Nd, we found $\sigma^{\mathrm{exp}}(\gamma, 1\mathrm{nX})$ was overestimated and $\sigma^{\mathrm{exp}}(\gamma, 2\mathrm{nX})$ was underestimated, consistent with the conclusion of Varlamov. However, the results of ^{142,143}Nd are inconsistent with the conclusion of Varlamov. In the present study, the influence of target uncertainty was considered, and the data of ^{143}Nd were corrected. These results examine the conclusions reported in the study by Varlamov and provide guidance for future high-precision measurements of photoneutron cross sections in the Nd isotopic chain using new γ -ray sources.

The theoretical–experimental method for evaluating is introduced in Sect. 2. The experimental data and new evaluation obtained are analyzed in Sect. 3. The uncertainty between them is discussed in Sect. 4. Finally, the conclusions and perspectives are given in Sect. 5.

2 Method

2.1 The experimental–theoretical method

An experimental–theoretical method independent of neutron multiplicity sorting was proposed in Ref. [28, 29] to obtain partial photoneutron cross sections free of systematic uncertainties. The method is based on using neutron yield reaction cross section $\sigma(\gamma, x\mathrm{n})$ data as the initial experimental information,

$$\begin{aligned}\sigma_{xn} &= \sigma(\gamma, x\mathrm{n}) \\ &= \sigma(\gamma, 1\mathrm{n}) + \sigma(\gamma, \mathrm{np}) + \sigma(\gamma, \mathrm{n}\alpha) + \cdots \\ &+ 2\sigma(\gamma, 2\mathrm{n}) + 2\sigma(\gamma, 2\mathrm{np}) + 2\sigma(\gamma, 2\mathrm{n}\alpha) + \cdots \\ &= \sum_i i\sigma_{i\mathrm{nX}},\end{aligned} \tag{1}$$

and for the total photoneutron reaction cross section $\sigma(\gamma, s\mathrm{n})$,

$$\begin{aligned}\sigma_{sn} &= \sigma(\gamma, s\mathrm{n}) \\ &= \sigma(\gamma, 1\mathrm{n}) + \sigma(\gamma, \mathrm{np}) + \sigma(\gamma, \mathrm{n}\alpha) + \cdots \\ &+ \sigma(\gamma, 2\mathrm{n}) + \sigma(\gamma, 2\mathrm{np}) + \sigma(\gamma, 2\mathrm{n}\alpha) + \cdots \\ &= \sum_i \sigma_{i\mathrm{nX}}.\end{aligned} \tag{2}$$

T. Kawano et al. [23] pointed out when the emission of charged particles is negligible in experimental photonuclear reaction, the measured one-neutron emission cross section is identical to that for the production of the $(Z, A-1)$ nucleus. In this case, the measured one-neutron emission cross section $\sigma(\gamma, 1\mathrm{nX})$,

$$\begin{aligned}\sigma_{1\mathrm{nX}} &= \sigma(\gamma, 1\mathrm{nX}) \\ &= \sigma(\gamma, 1\mathrm{n}) + \sigma(\gamma, \mathrm{np}) + \sigma(\gamma, \mathrm{n}\alpha) + \ldots,\end{aligned} \tag{3}$$

where X stands for anything except i-neutrons.

Figure 1 compares the theoretical and experimental data of $\sigma(\gamma, 1\mathrm{nX})$ and $\sigma(\gamma, 2\mathrm{nX})$ for ^{144}Nd. The experimental data were obtained using quasimonoenergetic annihilation photons and a Gd liquid scintillation detector at the Saclay laboratory, while the theoretical data were calculated using the modern Hauser-Feshbach nuclear reaction code TALYS (version 1.96) [30]. The discrepancy between the theoretical and experimental data may originate from substantial systematic uncertainties associated with the neutron multiplicity sorting method employed at Saclay.

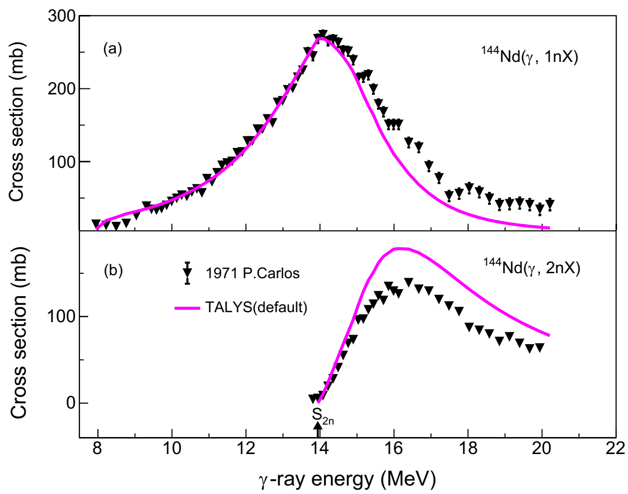

Fig. 1 (Color online) (**a**) $(\gamma, 1nX)$ reaction, (**b**) $(\gamma, 2nX)$ reaction. Comparison of the experimental cross sections for ^{144}Nd measured at the Saclay laboratory with TALYS calculations using default parameters

Due to these systematic uncertainties, Varlamov et al. [29] introduced the transition multiplicity function F_i, defined as a reliability criterion for partial photoneutron cross sections in the form of a ratio,

$$F_i = \frac{\sigma(\gamma, inX)}{\sigma_{xn}}, \tag{4}$$

to facilitate the evaluation of the experimental partial photoneutron cross sections.

According to Eq. (4), values such as $F_1 > 1.0$ or $F_2 > 0.50$ cannot be considered reliable. F_i values larger than the mentioned top limits indicate that the experimental sorting of neutrons between partial reactions has been carried out with large systematic uncertainties; therefore, the obtained reaction cross sections are not reliable. It should also be emphasized that, because F_i is defined purely as a ratio of cross sections, its values must always be positive.

The evaluated partial photoneutron cross sections $\sigma^{\rm eval}(\gamma, inX)$ are obtained by multiplying the experimental photoneutron yield cross section $\sigma^{\rm exp}(\gamma, xn)$ given in Eq. (1) by the theoretical functions $F_i^{\rm th}$ computed with the theoretical code,

$$\sigma^{\rm eval}(\gamma, inX) = F_i^{th}\sigma^{\rm exp}(\gamma, xn) = \frac{\sigma^{\rm th}(\gamma, inX)}{\sigma^{\rm th}(\gamma, xn)}\sigma^{\rm exp}(\gamma, xn), \tag{5}$$

where the $\sigma^{\rm th}(\gamma, xn)$ is the theoretical photoneutron yield cross section, and the $\sigma^{\rm th}(\gamma, inX)$ is the theoretical partial photoneutron reaction cross section.

The differences between the experimental and the evaluated cross sections were determined separately for reactions $(\gamma, 1nX)$ and $(\gamma, 2nX)$,

$$\Delta\sigma_1 = \Delta(\gamma, 1nX) = \sigma^{\rm exp}(\gamma, 1nX) - \sigma^{\rm eval}(\gamma, 1nX), \tag{6}$$

$$\Delta\sigma_2 = \Delta(\gamma, 2nX) = \sigma^{\rm exp}(\gamma, 2nX) - \sigma^{\rm eval}(\gamma, 2nX). \tag{7}$$

In Refs. [31–36], the experimental partial photoneutron cross sections obtained by quasimonoenergetic annihilation photons of many atomic nuclei (^{90,91,92,94}Zr, ^{115}In, $^{112-124}$Sn, ^{159}Tb, ^{186,188,189,190,192}Os, ^{208}Pb, etc.) were analyzed using an experimental–theoretical method and obtained new evaluation data.

2.2 γ strength function models

The key to obtaining the theoretical F_i values is to determine the photoneutron yield cross sections of $^{142-146,148,150}$Nd. These cross sections were calculated with common classical γ strength function models in TALYS, and the results were compared by means of χ^2 analysis,

$$\chi^2 = \frac{1}{N}\Sigma\frac{(\sigma_{\rm th} - \sigma_{\rm exp})^2}{\sigma_{\rm err}^2}, \tag{8}$$

where N is the total number of experimental points, $\sigma_{\rm th}$, $\sigma_{\rm exp}$, and $\sigma_{\rm err}$ are the theoretical value of the neutron yield cross sections, the experimental measurement value of the neutron yield cross sections, and the uncertainty of the experimental measurement value, respectively.

The theoretical photoneutron yield cross sections $\sigma(\gamma, xn)$ of ^{144}Nd, calculated using Eq. (1), are shown in Fig. 2, along with the experimental data [37–47]. γ-ray strength functions play a crucial role in describing transitions involving γ rays in nuclear reactions [48, 49]. Figure 2 demonstrates that the choice of γ-ray strength function has a considerable impact on the calculated photoneutron yield cross sections.

As shown in Fig. 3, for $A \geq 145$, the Brink–Axel Lorentzian (BAL) model is very close to Goriely's T-dependent HF model and Goriely's hybrid model, while for $A \leq 143$, the BAL and the SMLO models describe the data equally well. The BAL model generally results in the lowest χ^2 values over all isotopes, with only a minor deviation at $A = 150$, where Goriely's hybrid model performs marginally better. The average χ^2 value obtained using the BAL model is 11.41. To ensure consistent and systematic treatment across the entire isotopic chain, the BAL model was adopted in the present analysis. A quantitative comparison shows that the average relative deviations in neutron multiplicity functions (F_1, F_2) between other γSF models and BAL are 10.60% 12.53% 10.69% 9.21% 8.79% 13.59% 7.37% 6.86% and 10.15% for models 1 through 10 (excluding 2), indicating that moderate differences exist among the models and warrant consideration in model-based evaluations.

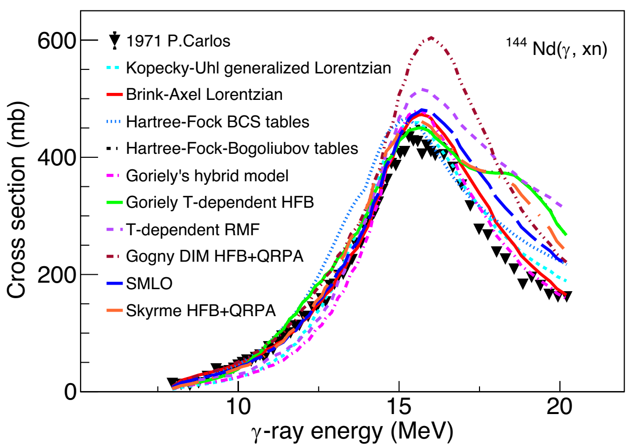

Fig. 2 (Color online) The experimental photoneutron yield cross sections $\sigma(\gamma, xn)$ of ^{144}Nd obtained at Saclay laboratory and compared with the ten γ strength function models calculations in TALYS (1, Kopecky-Uhl generalized Lorentzian [37], 2, Brink–Axel Lorentzian [38, 39], 3, Hartree–Fock–Bogoliubov tables [40], 4, Hartree–Fock BCS tables [41], 5, Goriely's hybrid model [42], 6, Goriely T-dependent HFB [43], 7, T-dependent RMF [44], 8, Gogny DIM HFB+QRPA [45], 9, SMLO [46], 10, Skyrme HFB+QRPA [47])

The Brink–Axel Lorentzian model is based on the Brink–Axel hypothesis [50], which states that the photon absorption cross section is independent of the excitation energy of a nuclear system and is an assumption used in nuclear structure studies and calculations. This model offers a solid theoretical basis for our analysis, balancing the reliability and precision of neutron interaction modeling.

The parameters of γ-strength function models for each nuclide are listed in Table 1, where E, Γ, and σ are the energy center value, width, and strength of the formant, respectively.

Using the Brink–Axel Lorentzian model in TALYS, the theoretical neutron multiplicity functions F_i^{th} were obtained using Eq. (4) and are shown in Fig. 4. These results were compared with the experimental neutron multiplicity functions F_i^{exp} derived from the ^{144}Nd data measured at the Saclay laboratory.

Up to the $(\gamma, 2\text{nX})$ reaction threshold of $S_{2n} = 13.94$ MeV, F_1^{th} remains equal to 1. Once the $(\gamma, 2\text{nX})$ channel opens, F_1^{th} diminishes in correspondence with the competition from the growing $\sigma(\gamma, 2\text{nX})$ and shrinking $\sigma(\gamma, 1\text{nX})$ cross sections, eventually approaching zero.

There is a clear discrepancy between the experimental and calculated values of F_1 and F_2. The F_i^{exp} value is consistent with F_i^{th} value only when the γ energies are below the two-neutron separation energy $S_{2\text{n}}$. For γ energies above $S_{2\text{n}}$, the F_1^{exp} shows an overestimated trend and F_2^{exp} shows an underestimated trend. This suggests that in the Saclay (γ, xn) measurements of Nd isotopes, $(\gamma, 2\text{nX})$ events may have been erroneously classified as $(\gamma, 1\text{nX})$ events.

3 Result

After F_i is determined, the evaluated value of the photoneutron reaction cross section can be calculated using Eq. (5). $\sigma^{\text{eval}}(\gamma, i\text{nX})$ for Nd isotopes are displayed in the following

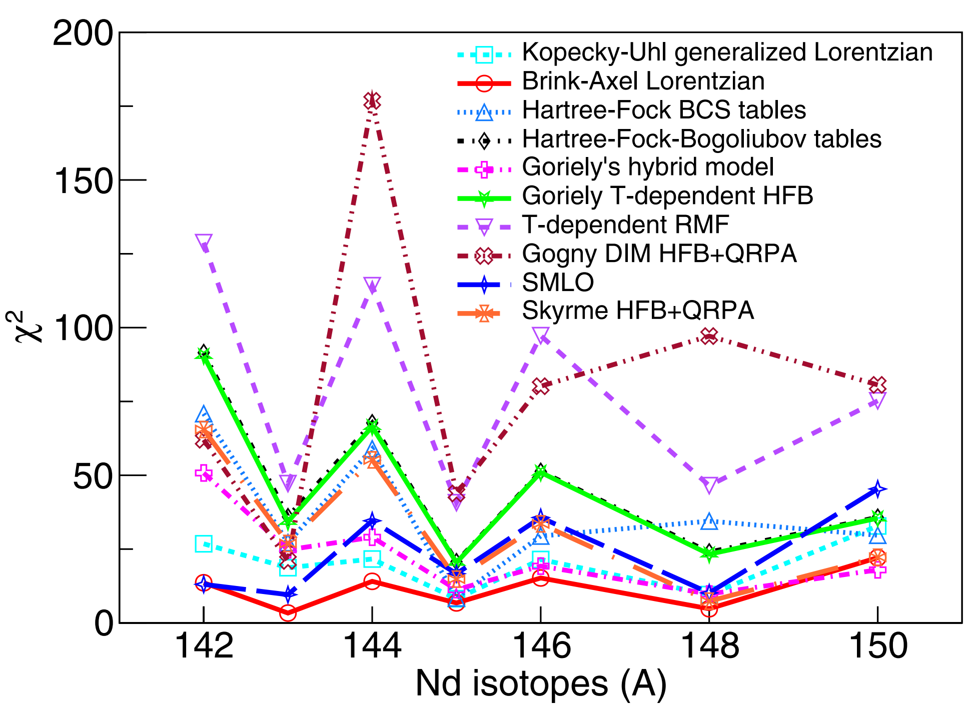

Fig. 3 (Color online) The χ^2 values obtained with the experimental photoneutron yield cross sections $\sigma(\gamma, xn)$ and compared with the ten γ strength function models in TALYS

Table 1 Photoneutron yield model parameters for $^{142-146,148,150}$Nd in TALYS with Brink–Axel Lorentzian model

Nuclide	E (MeV)	Γ (MeV)	σ (mb)
^{142}Nd	14.94	4.44	359.00
^{143}Nd	15.01	4.75	349.00
^{144}Nd	15.05	5.28	317.00
^{145}Nd	14.95	6.31	296.00
^{146}Nd	14.74	5.78	310.00
^{148}Nd	12.76	3.97	220.00
	15.48	5.30	107.00
^{150}Nd	12.30	3.38	175.00
	16.04	5.17	223.00

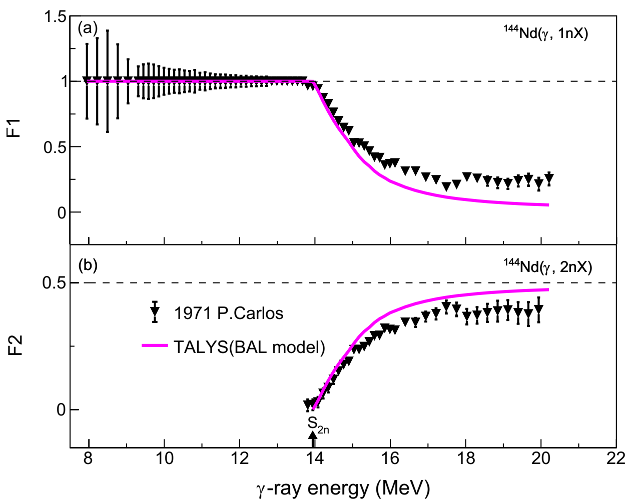

Fig. 4 (Color online) The experimental neutron multiplicity functions F_1 (**a**) and F_2 (**b**) for the isotope ^{144}Nd, obtained from data measured at the Saclay laboratory, are compared with TALYS calculations performed with default parameters, except that the γ strength function was chosen by the BAL model

paragraph. The results can be classified based on the comparison between $\sigma^{\text{exp}}(\gamma, i\text{nX})$ and $\sigma^{\text{eval}}(\gamma, i\text{nX})$ at energies above the two-neutron threshold S_{2n}. (A) In most energy regions (approximately 90%), case of $\Delta\sigma_2 \leq 0$ is satisfied, as observed for $^{144-146,148,150}$Nd; (B) In most energy regions (approximately 90%), case of $\Delta\sigma_2 \geq 0$ is satisfied, as observed for ^{143}Nd; (C) For some energies, case (A) is satisfied, while for some energies, case (B) is satisfied, as observed for ^{142}Nd. While case (A) is consistent with Varlamov's conclusion, cases (B) and (C) diverge from his expectations.

3.1 Evaluation of isotopes $^{144-146,148,150}$Nd

For the isotope ^{144}Nd, a comparison between $\sigma^{\text{eval}}(\gamma, i\text{nX})$, $\sigma^{\text{exp}}(\gamma, i\text{nX})$ and the existing evaluation data is shown in Fig. 5. Figure 5a and b indicates the comparison of ^{144}Nd $(\gamma, 1\text{nX})$ reaction and ^{144}Nd $(\gamma, 2\text{nX})$ reaction, respectively. Figure 5c shows that the values of $\sigma^{\text{exp}}(\gamma, i\text{nX}) - \sigma^{\text{eval}}(\gamma, i\text{nX})$. The integrated cross section σ^{int} containing the energy ranges of only 1n and 1n + 2n is obtained and presented in Table 2.

The average relative deviations (ARD) between the experimental/evaluated results and the cross sections from nuclear data libraries are defined as

$$\text{ARD}_1 = \frac{1}{n}\sum_{i=1}^{n}\frac{|\sigma_{\text{lib}} - \sigma_{\text{exp}}|}{|\sigma_{\text{exp}}|}, \tag{9}$$

$$\text{ARD}_2 = \frac{1}{n}\sum_{i=1}^{n}\frac{|\sigma_{\text{lib}} - \sigma_{\text{eval}}|}{|\sigma_{\text{eval}}|}. \tag{10}$$

Here, n denotes the number of experimental points, σ_{exp} is the experimental cross section, σ_{eval} is the evaluated cross section obtained in this study, and σ_{lib} represents the cross

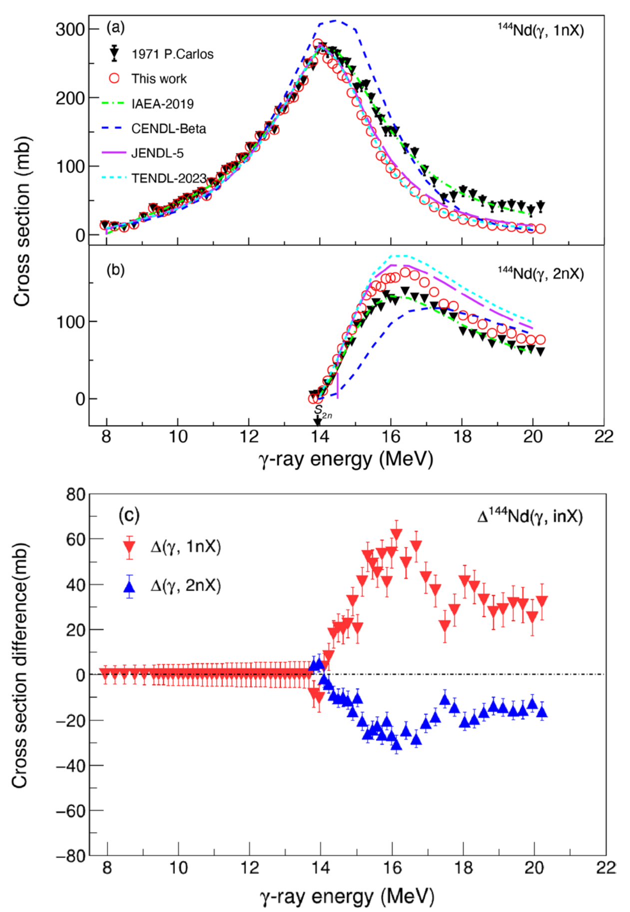

Fig. 5 (Color online) The comparison between $\sigma^{\text{eval}}(\gamma, i\text{nX})$, $\sigma^{\text{exp}}(\gamma, i\text{nX})$ and the existing evaluation data; **a** the case of ^{144}Nd $(\gamma, 1\text{nX})$ reaction; **b** the case of ^{144}Nd $(\gamma, 2\text{nX})$ reaction; **c** the values of differences $\Delta\sigma_i, i = 1, 2$

Table 2 The integrated σ^{int} of evaluated cross sections of total and partial photoneutron reactions for various reactions on ^{144}Nd nucleus, compared to experimental data at Saclay laboratory

Reaction	σ^{int}_{exp} (mb)	σ^{int}_{eval} (mb)
$E^{int} = 7.95–13.80$ MeV		
$(\gamma, x\text{n})$	532.99	532.99
$(\gamma, s\text{n})$	532.70	532.99
$(\gamma, 1\text{nX})$	532.40	532.99
$E^{int} = 7.95–20.21$ MeV		
$(\gamma, x\text{n})$	2444.75	2444.75
$(\gamma, s\text{n})$	1881.16	1774.12
$(\gamma, 1\text{nX})$	1317.58	1103.48
$(\gamma, 2\text{nX})$	563.28	670.62

section values from the evaluated nuclear data libraries. The effectiveness level of the present evaluation is defined as the difference between the two ARD values, let $effectiveness\ level = \text{ARD}_1 - \text{ARD}_2$.

As shown in Fig. 5a and b, for the isotope ^{144}Nd, compared with the Saclay measurements $\sigma^{exp}(\gamma, i\text{nX})$, the evaluated cross sections $\sigma^{eval}(\gamma, i\text{nX})$ show improved consistency with JENDL-5, CENDL-Beta, and TENDL-2023, whereas their agreement with IAEA-2019 is comparatively poorer. These results demonstrate the effectiveness of the proposed evaluation method. For $(\gamma, 1\text{nX})$ case, the effectiveness levels for databases of JENDL-5, CENDL-Beta, TENDL-2023, and IAEA-2019 are 3.75%, −5.52%, 14.11%, and −37.21% respectively. For $(\gamma, 2\text{nX})$ case, the effectiveness levels are 22.76%, 3.27%, −27.74%, and −67.67%, respectively.

The differences between the evaluated and experimental cross sections were determined separately for the reactions $(\gamma, 1\text{nX})$ and $(\gamma, 2\text{nX})$, as shown in Fig. 5c. At energies below the threshold $S_{2\text{n}}$ of reaction $(\gamma, 2\text{nX})$, where there is little problem in neutron multiplicity sorting, the difference between the experimental and theoretical integrated cross section $\sigma(\gamma, 1\text{nX})$ is only 0.05% (532.70 mb and 532.40 mb, respectively). But at high energies where reactions $(\gamma, 1\text{nX})$ and $(\gamma, 2\text{nX})$ compete with each other range 13.80 to 20.21 MeV, the data on both differ markedly: $\sigma^{int}_{eval}(\gamma, 1\text{nX}) = 570.08$ mb, which is 27% smaller than $\sigma^{int}_{exp}(\gamma, 1\text{nX})$ (784.88 mb). $\sigma^{int}_{eval}(\gamma, 2\text{nX}) = 670.62$ mb, which is 19% larger than $\sigma^{int}_{exp}(\gamma, 2\text{nX})$ (which is 563.28 mb). Such large and opposite-direction divergences between the cross sections of reactions $(\gamma, 1\text{nX})$ and $(\gamma, 2\text{nX})$ convincingly demonstrate the reasons for the substantial systematic uncertainties in the experiments at the Saclay laboratory, which are due to the unreliable transmission of a large number of neutrons from channel 2n to channel 1n.

Similar to the conclusions for ^{144}Nd, the evaluated cross section data for the $(\gamma, 1\text{nX})$ and $(\gamma, 2\text{nX})$ reactions of ^{145,146,148,150}Nd were compared with the corresponding experimental results and the values from the evaluated nuclear data libraries, as shown in Fig. 6. The relative differences between integrated $\sigma^{exp}(\gamma, 1\text{nX})$ and $\sigma^{eval}(\gamma, 1\text{nX})$ are 36%, 48%, 26%, 108%, respectively. For $(\gamma, 2\text{nX})$, the relative differences are 14%, 17%, 5%, 21%, respectively. The relative average differences between the evaluated cross sections and those from various nuclear data libraries (JENDL-5, TENDL-2023, IAEA-2019, and CENDL-Beta) also exhibited significant variation for ^{145,146,148,150}Nd. As shown in Table 3, consistent with the conclusions of ^{144}Nd isotope, for the isotopes ^{145,146,148,150}Nd, the values of $\sigma^{eval}(\gamma, i\text{nX})$ are closer to those of JENDL-5, CENDL-Beta, and TENDL-2023, whereas the experimental data $\sigma^{exp}(\gamma, i\text{nX})$ are more consistent with IAEA-2019.

3.2 Evaluation of isotope ^{143}Nd

For the isotope ^{143}Nd, a comparison between $\sigma^{eval}(\gamma, i\text{nX})$, $\sigma^{exp}(\gamma, i\text{nX})$ and the existing evaluation data is shown in Fig. 7. Figure 7a and b indicates the comparison of ^{143}Nd $(\gamma, 1\text{nX})$ reaction and ^{143}Nd $(\gamma, 2\text{nX})$ reaction, respectively. Figure 7c shows that the values of $\sigma^{exp}(\gamma, i\text{nX}) - \sigma^{eval}(\gamma, i\text{nX})$. The integrated cross section σ^{int} containing the energy ranges of only 1n and 1n + 2n is obtained and presented in Table 4. Because the experimental $(\gamma, 2\text{nX})$ cross section still exists at energies below the $S_{2\text{n}}$ threshold, the σ^{int}_{exp} of the $(\gamma, x\text{n})$ reaction is larger than that of the $(\gamma, 1\text{nX})$ reaction when $E^{int} = 9.31–15.71$ MeV.

As shown in Fig. 7a and b, a similar trend is observed for ^{143}Nd, where $\sigma^{eval}(\gamma, i\text{nX})$ shows closer agreement with JENDL-5, CENDL-Beta, and TENDL-2023 than with IAEA-2019 when compared to the experimental data $\sigma^{exp}(\gamma, i\text{nX})$. This further confirms the effectiveness of the evaluation method used in this study. For $(\gamma, 1\text{nX})$ case, the effectiveness levels for databases of JENDL-5, CENDL-Beta, TENDL-2023, and IAEA-2019 are 3.43%, 2.72%, 2.93%, and −1.55%, respectively. For $(\gamma, 2\text{nX})$ case, the effectiveness levels are 35.15%, 23.86%, 29.61%, and −67.91%, respectively.

The differences $\Delta\sigma$ between the experimental and evaluated cross sections [Fig. 7c] obtained for partial reactions seem to be 'mirrored'. Almost all values of $(\gamma, 1\text{nX})$ are negative, whereas those of $(\gamma, 2\text{nX})$ are positive. When the energy range 14.08–19.80 MeV, $\sigma^{exp} - \sigma^{eval}$ is opposite: $\sigma^{int}_{eval}(\gamma, 1\text{nX}) = 611.71$ mb, which is 16% greater than $\sigma^{int}_{exp}(\gamma, 1\text{nX})$ (which is 524.94 mb). $\sigma^{int}_{eval}(\gamma, 2\text{nX}) = 140.96$ mb, which is 20% smaller than $\sigma^{int}_{exp}(\gamma, 2\text{nX})$(which is 178.35 mb). For the isotope ^{143}Nd, it is interesting to find that $\Delta\sigma_1$ is greater than zero and $\Delta\sigma_2$ is less than zero at

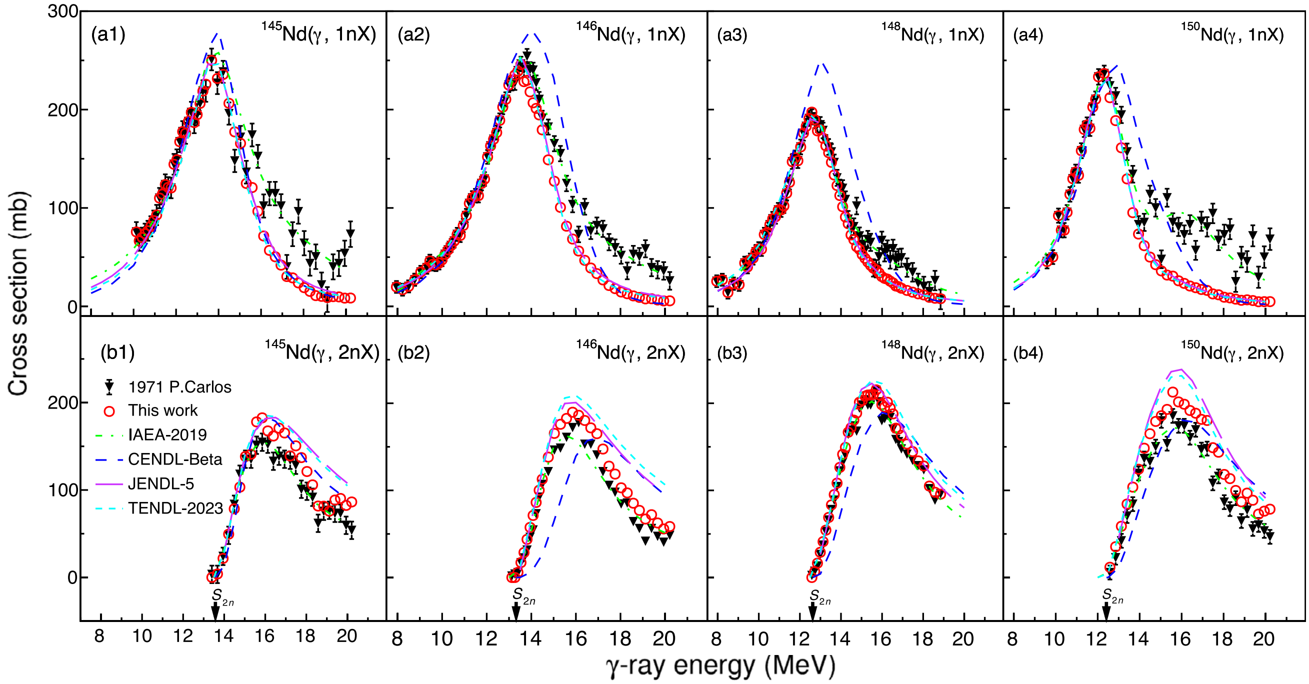

Fig. 6 (Color online) The comparison between $\sigma^{\mathrm{eval}}(\gamma, i\mathrm{nX})$, $\sigma^{\mathrm{exp}}(\gamma, i\mathrm{nX})$ and the existing evaluation data; **a1**–**a4** the case of ^{145,146,148,150}Nd $(\gamma, 1\mathrm{nX})$ reaction; **b1**–**b4** the case of ^{145,146,148,150}Nd $(\gamma, 2\mathrm{nX})$ reaction

these energies. However, the results at 18.71 MeV and 19.80 MeV exhibit opposite behaviors in $\Delta\sigma_1$ and $\Delta\sigma_2$.

3.3 Evaluation of isotope ^{142}Nd

For the isotope ^{142}Nd, a comparison between $\sigma^{\mathrm{eval}}(\gamma, i\mathrm{nX})$, $\sigma^{\mathrm{exp}}(\gamma, i\mathrm{nX})$ and the existing evaluation data is shown in Fig. 8. Figure 8a and b indicates the comparison of ^{142}Nd $(\gamma, 1\mathrm{nX})$ reaction and ^{142}Nd $(\gamma, 2\mathrm{nX})$ reaction, respectively. Figure 8c shows that the values of $\sigma^{\mathrm{exp}}(\gamma, i\mathrm{nX}) - \sigma^{\mathrm{eval}}(\gamma, i\mathrm{nX})$. The integrated cross sections σ^{int} for the energy ranges of only $1n$ and $1n + 2n$ are obtained and presented in Table 5. Similar to ^{142}Nd, since the experimental $(\gamma, 2\mathrm{n})$ cross sections were still measured below the $S_{2\mathrm{n}}$ threshold, the $\sigma^{\mathrm{int}}_{\mathrm{exp}}$ of the $(\gamma, x\mathrm{n})$ reaction is larger than that of the $(\gamma, 1\mathrm{nX})$ reaction when $E^{\mathrm{int}} = 9.85{-}17.75$ MeV.

As shown in Fig. 8a and b, for the isotope ^{142}Nd, the evaluated cross sections $\sigma^{\mathrm{eval}}(\gamma, i\mathrm{nX})$ exhibit improved agreement with all four major nuclear data libraries compared with the experimental data $\sigma^{\mathrm{exp}}(\gamma, i\mathrm{nX})$. These results provide further evidence of the applicability of the evaluation method. For $(\gamma, 1\mathrm{nX})$ case, the effectiveness levels for databases of JENDL-5, CENDL-Beta, TENDL-2023, and IAEA-2019 are 0.64%, −2.21%, 0.95%, and 0.67%, respectively. For $(\gamma, 2\mathrm{nX})$ case, the effectiveness levels are 43.15%, 13.61%, 38.71%, and 12.90%, respectively.

As shown in Fig. 8c and Table 5, the values of $\sigma^{\mathrm{eval}}(\gamma, i\mathrm{nX})$ are very close to $\sigma^{\mathrm{exp}}(\gamma, i\mathrm{nX})$ when the γ-ray energy is lower than 17.75 MeV. When the energy is between 17.75 and 20.21 MeV, $\sigma^{\mathrm{int}}_{\mathrm{eval}}(\gamma, 1\mathrm{nX}) = 205.65$ mb which is 9% smaller than $\sigma^{\mathrm{int}}_{\mathrm{exp}}(\gamma, 1\mathrm{nX})$ (226.08 mb). $\sigma^{\mathrm{int}}_{\mathrm{eval}}(\gamma, 2\mathrm{nX}) = 53.36$ mb, which is 14% larger than $\sigma^{\mathrm{int}}_{\mathrm{exp}}(\gamma, 2\mathrm{nX})$ (46.53 mb). Notably, as shown in Fig. 8c, the values of $\Delta\sigma_1$ are less than zero before 18.57 MeV

Table 3 Variations in the average relative deviations of experimental cross sections $\sigma^{\mathrm{exp}}(\gamma, i\mathrm{nX})$ and evaluated cross sections $\sigma^{\mathrm{eval}}(\gamma, i\mathrm{nX})$ with respect to IAEA-2019, JENDL-5, CENDL-Beta, and TENDL-2023, $i = 1, 2$

	IAEA-2019		JENDL-5		CENDL-Beta		TENDL-2023	
	$(\gamma, 1\mathrm{nX})$	$(\gamma, 2\mathrm{nX})$	$(\gamma, 1\mathrm{nX})$	$(\gamma, 2\mathrm{nX})$	$(\gamma, 1\mathrm{nX})$	$(\gamma, 2\mathrm{nX})$	$(\gamma, 1\mathrm{nX})$	$(\gamma, 2\mathrm{nX})$
^{145}Nd	−62.4%	−2.48%	8.39%	20.06%	16.92%	19.22%	16.12%	21.56%
^{146}Nd	−6.12%	−5.53%	7.02%	35.58%	0.75%	19.02%	13.05%	39.93%
^{148}Nd	−21.95%	0.98%	13.20%	7.91%	−10.87%	1.97%	14.14%	8.77%
^{150}Nd	−161.89%	−0.54%	31.97%	30.34%	−9.33%	12.37%	34.13%	32.75%

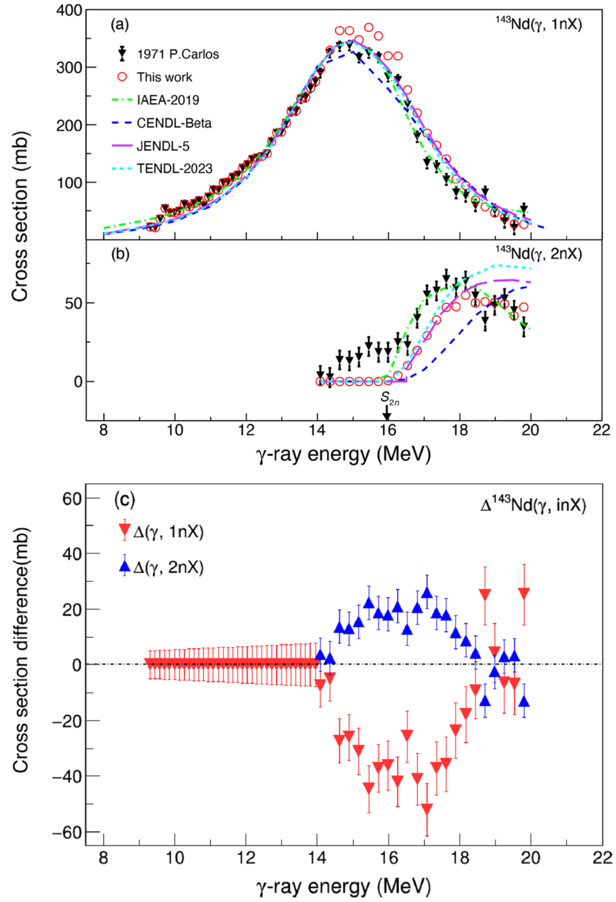

Fig. 7 (Color online) The comparison between $\sigma^{\text{eval}}(\gamma, i\text{nX})$, $\sigma^{\text{exp}}(\gamma, i\text{nX})$ and the existing evaluation data; **a** the case of ^{143}Nd $(\gamma, 1\text{nX})$ reaction; **b** the case of ^{143}Nd $(\gamma, 2\text{nX})$ reaction; **c** the values of differences $\Delta\sigma_i$, $i = 1, 2$

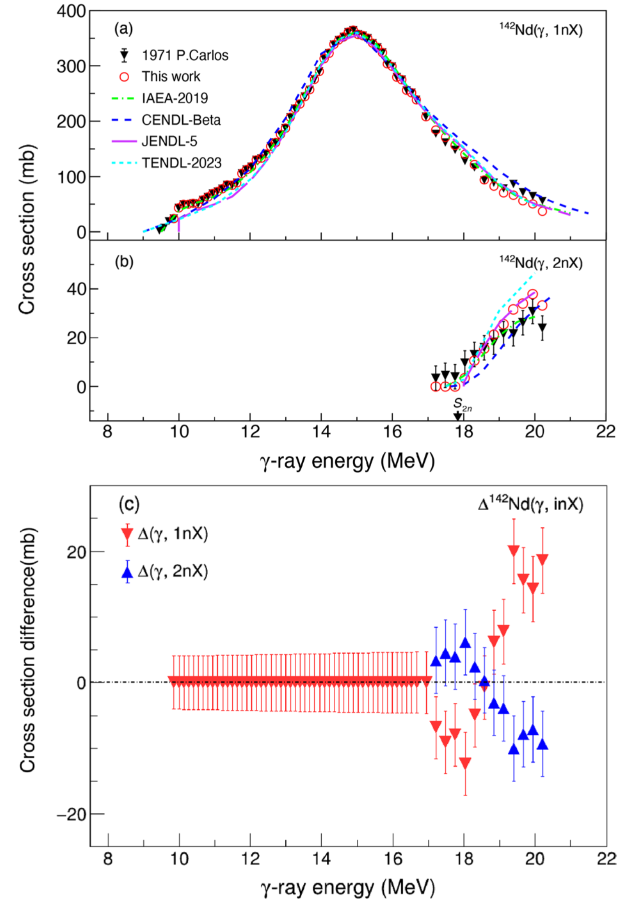

Fig. 8 (Color online) The comparison between $\sigma^{\text{eval}}(\gamma, i\text{nX})$, $\sigma^{\text{exp}}(\gamma, i\text{nX})$ and the existing evaluation data; **a** the case of ^{142}Nd $(\gamma, 1\text{nX})$ reaction; **b** the case of ^{142}Nd $(\gamma, 2\text{nX})$ reaction; **c** the values of differences $\Delta\sigma_i$, i= 1, 2

Table 4 The integrated σ^{int} of evaluated cross sections of total and partial photoneutron reactions for various reactions on ^{143}Nd nucleus, compared to experimental data at Saclay laboratory

Reaction	$\sigma^{\text{int}}_{\text{exp}}$ (mb)	$\sigma^{\text{int}}_{\text{eval}}$ (mb)
$E^{\text{int}} = 9.31$–15.71 MeV		
$(\gamma, x\text{n})$	1178.26	1178.26
$(\gamma, s\text{n})$	1156.75	1178.26
$(\gamma, 1\text{nX})$	1135.24	1178.26
$E^{\text{int}} = 9.31$–19.80 MeV		
$(\gamma, x\text{n})$	2070.05	2070.05
$(\gamma, s\text{n})$	1865.11	1929.01
$(\gamma, 1\text{nX})$	1660.18	1787.97
$(\gamma, 2\text{nX})$	178.35	140.96

Table 5 The integrated σ^{int} of evaluated cross sections of total and partial photoneutron reactions for various reactions on ^{142}Nd nucleus, compared to experimental data at Saclay laboratory

Reaction	$\sigma^{\text{int}}_{\text{exp}}$ (mb)	$\sigma^{\text{int}}_{\text{eval}}$ (mb)
$E^{\text{int}} = 9.85$–17.75 MeV		
$(\gamma, x\text{n})$	1602.90	1602.90
$(\gamma, s\text{n})$	1600.19	1602.90
$(\gamma, 1\text{nX})$	1597.48	1602.90
$E^{\text{int}} = 9.85$–20.21 MeV		
$(\gamma, x\text{n})$	1922.05	1922.05
$(\gamma, s\text{n})$	1872.80	1862.05
$(\gamma, 1\text{nX})$	1823.56	1808.55
$(\gamma, 2\text{nX})$	46.53	53.36

and greater and becomes positive above this energy. The situation for $\Delta\sigma_2$ is the opposite.

4 Discussion

As shown in the above results, the evaluations of $^{144-146,148,150}$Nd are consistent with the conclusion of Varlamov, and the difference between σ^{eval} and σ^{exp} is primarily attributed to detector uncertainty [18, 51]. Meanwhile, some results different from Varlamov's expectations were also discovered, such as the results of ^{142,143}Nd. In these cases, the reason for the difference between σ^{eval} and σ^{exp} may also originate from the isotopic target impurity.

Isotope targets in the oxide form were used for measurements at the Saclay laboratory. The target materials contained isotope impurities, the parameters of which are provided in [10]. First, the impurity thresholds should be checked to determine whether they may influence the measured results. For $(\gamma, 1\text{nX})$, if the 1n threshold is lower than the γ-ray energy($S_\text{n}(i) < E$, where $i = 1, 2, ...$ denotes the impurities), the effect of the impurity should be considered; for $(\gamma, 2\text{nX})$, if $S_{2\text{n}}(i) < E$, the effect of the impurity should also be considered. Subsequently, the measured cross sections were refined by subtracting the contributions from those isotopes within the reaction threshold region (S_n and $S_{2\text{n}}$),

$$\sigma_B = \frac{\sigma_{\text{total}} - x\,\sigma_A}{y} \tag{11}$$

where σ_{total} is the total measured photoneutron cross section of the sample, σ_A is the known cross section of element A, and x and y are the relative isotopic abundances of elements A and B in the target material, respectively.

The experimental results of eliminating isotope impurities were re-evaluated, and the $\Delta\sigma_1$ and $\Delta\sigma_2$ are shown in Fig. 9. (a), (b) and (c) represent case(a), case(b), and case(c), respectively, in the results section. The purity of the target had little effect on case(a) and case(c). This is because the photoneutron cross sections of their impurities are similar, and the content is relatively low. It can be seen that within the energy range of 1–2 MeV greater than the $S_{2\text{n}}$ threshold, the trends of $\Delta\sigma_1$ and $\Delta\sigma_2$ are exactly opposite to those in the higher energy region, but their values are within the experimental uncertainty range, as shown by the red band in Fig. 9. This may reflect the measurement uncertainties arising from the limited accuracy near the $S_{2\text{n}}$ threshold.

As shown in Fig. 9, after eliminating the influence of impurities in the target ^{143}Nd (case (b)), the absolute values of $\Delta\sigma_1$ and $\Delta\sigma_2$ decreased significantly, and more than 80% were within the experimental uncertainty range. Therefore, the influence of target purity must be fully considered in experiments and evaluations. Meanwhile, other factors, including detector efficiency and accidental coincidence events, should be fully considered to resolve such discrepancies.

Considering these factors, it is effective to employ quasi-monochromatic γ-ray beams generated via laser Compton scattering (LCS) [52, 53] in combination with flat-efficiency detectors [54, 55], as this approach is expected to minimize the observed discrepancies and provide more accurate measurements. For example, ongoing research at the SLEGS facility [56–61] is advancing this objective, while the establishment of the ELI-NP facility is expected to lead to new and more precise measurements [62, 63]

5 Summary

The experimental data for $^{142-146,148,150}$Nd, measured at the Saclay laboratory using a modified photoneutron multiplicity sorting method, were evaluated and corrected. The evaluated physical criteria $F_i = \sigma(\gamma, i\text{n})/\sigma(\gamma, x\text{n})$ based on the experimental neutron yield cross sections $\sigma^{\text{exp}}(\gamma, x\text{n})$ are independent of the neutron multiplicity sorting problem, and the equations of the theoretical model in TALYS were used to analyze the systematic uncertainties present in

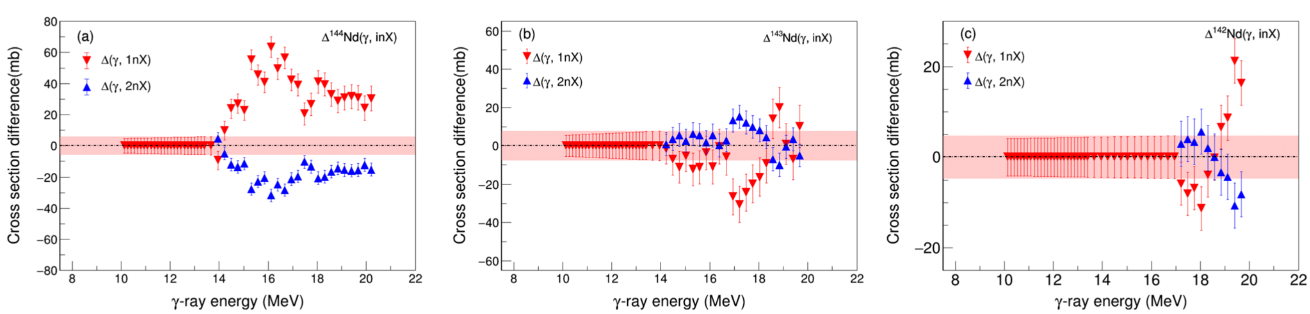

Fig. 9 (Color online) The differences between the experimental and the evaluated cross sections after correction for isotopic impurities: **a** the case of ^{142}Nd, **b** the case of ^{143}Nd, **c** the case of ^{144}Nd

the experimental cross sections. An experimental–theoretical method for the evaluation of partial reaction cross sections was used to determine new cross sections for reactions (γ, 1nX) and (γ, 2nX) on $^{142-146,148,150}$Nd. The newly evaluated data are in reasonable agreement with the JENDL-5 and TENDL-2023 libraries.

The results show that the conclusions for $^{142,144-146,148,150}$Nd are consistent with those of Varlamov, whereas ^{143}Nd exhibits significant deviations from them. In this study, detector uncertainty and target purity were considered, and appropriate corrections were applied. Consequently, the absolute values of $\Delta\sigma_1$ and $\Delta\sigma_2$ were substantially reduced, with more than 80% falling within the experimental uncertainty range. Therefore, the influence of isotopic target impurities must be fully considered in experimental measurements and data evaluations. Meanwhile, there are still some other factors, including the detector efficiency and accidental coincidence events, that need to be further studied. The conclusion of this study is helpful for photoneutron reaction experiments carried out on LCS γ-ray sources.

Acknowledgements We would like to express our gratitude to Prof. M. Itoh, Dr. S. Adachi, and Mr. B.M.G. Chew from Tohoku University for their guidance and suggestions during the revision process.

Author Contributions All authors contributed to the study conception and design. Material preparation, data collection and analysis were performed by Yu-Long Shen, Zhi-Cai Li, Ting-Kai Ma, Wen-Yu Tan, Ting Wu, Xin-Xiang Li, Ji-Min Wang, Xi Tao, Gong-Tao Fan, Rui-Rui Xu, and Wen Luo. The first draft of the manuscript was written by Yu-Long Shen, and all authors commented on previous versions of the manuscript. All authors read and approved the final manuscript.

Data Availability The data that support the findings of this study are openly available in Science Data Bank at https://cstr.cn/31253.11.sciencedb.j00186.00969 and https://doi.org/10.57760/sciencedb.j00186.00969.

Declarations

Conflict of interest The authors declare that they have no conflict of interest.

References

1. B.M. Spicer, The giant dipole resonance. Adv. Nucl. Phys. **2**, 1–78 (1969). https://doi.org/10.1007/978-1-4684-8343-7_1
2. Z.X. Zhang, K.X. Li, Q.L. Wei et al., Simulation study of medical isotope production using electron accelerator-driven photoneutron source. Nuclear Tech. **47**(9), 090203 (2024). https://doi.org/10.11889/j.0253-3219.2024.hjs.47.090203
3. A. Zilges, D.L. Balabanski, J. Isaak et al., Photonuclear reactions-From basic research to applications. Prog. Part. Nucl. Phys. **122**, 103903 (2022). https://doi.org/10.1016/j.ppnp.2021.103903
4. X.Y. Sun, W. Luo, H.Y. Lan et al., Transmutation of long-lived fission products in an advanced nuclear energy system. Sci. Rep. **12**, 2240 (2022). https://doi.org/10.1038/s41598-022-06344-y
5. D.L. Balabanski, W. Luo, Nuclear photonics and nuclear isomers. Eur. Phys. J. Sp. Top. **233**, 1161–1179 (2024). https://doi.org/10.1140/epjs/s11734-024-01132-3
6. Z.R. Hao, G.T. Fan, H.W. Wang et al., The day-one experiment at SLEGS: systematic measurement of the (γ, 1n) cross sections on ^{197}Au and ^{159}Tb for resolving existing data discrepancies. Sci. Bull. **70**, 2591–2597 (2025). https://doi.org/10.1016/j.scib.2025.05.037
7. Z.C. Li, Y.X. Yang, Z.W. Cao et al., Effective extraction of photoneutron cross-section distribution using gamma activation and reaction yield ratio method. Nucl. Sci. Tech. **34**, 170 (2023). https://doi.org/10.1007/s41365-023-01330-z
8. Z.C. Li, Z.R. Hao, Q.K. Sun et al., New measurement of ^{63}Cu(γ, n)^{62}Cu cross section using a quasi-monoenergetic γ-ray beam. Nucl. Sci. Tech. **36**, 34 (2025). https://doi.org/10.1007/s41365-024-01631-x
9. Y.N. Gu, W.J. Zhao, X.G. Cao et al., Feasibility study of the photonuclear reaction cross section of medical radioisotopes using a laser Compton scattering gamma source. Nucl. Sci. Tech. **35**, 155 (2024). https://doi.org/10.1007/s41365-024-01481-7
10. P. Carlos, H. Beil, R. Bergere et al., The giant dipole resonance in the transition region for the neodymium isotopes. Nucl. Phys. A **172**, 437–448 (1971). https://doi.org/10.1016/0375-9474(71)90725-1
11. B.L. Berman, S. Fultz, Measurements of the giant dipole resonance with monoenergetic photons. Rev. Mod. Phys. **47**(3), 713 (1975). https://doi.org/10.1103/RevModPhys.47.713
12. S.S. Dietrich, B.L. Berman, Atlas of photoneutron cross sections obtained with monoenergetic photons. At. Data Nucl. Data Tables **38**, 199–338 (1988). https://doi.org/10.1016/0092-640X(88)90033-2
13. A.V. Varlamov, V.V. Varlamov, D.S. Rudenko et al., in *and International Atomic Energy Agency, International Nuclear Data Committee, Vienna (Austria)* (Parameters and Graphs of Photonuclear Reaction Cross Sections. IAEA, Atlas of Giant Dipole Resonances, 1999)
14. A. Veyssiére, H. Beil, R. Bergère et al., Photoneutron cross sections of ^{208}Pb and ^{197}Au. Nucl. Phys. A **159**, 561–576 (1970). https://doi.org/10.1016/0375-9474(70)90727-X
15. A. Veyssière, Design and construction of a Faraday cup for measuring small electron currents. CEA Saclay, 91 - Gif-sur-Yvette (France), (1967)
16. Russia Lomonosov Moscow State University Skobeltsyn Institute of Nuclear Physics Centre for Photonuclear Experiments Data database Nuclear Reaction Database (EXFOR), http://cdfe.sinp.msu.ru/exfor/index.php International Atomic Energy Agency Nuclear Data Section database Experimental Nuclear Reaction Data (EXFOR), http://www-nds.iaea.org/exforhttp://www.nndc.bnl.gov/exfor/exfor00.htm USA National Nuclear Data Center database CSISRS and EXFOR Nuclear Reaction Experimental Data
17. V.V. Varlamov, B. Ishkhanov, V. Orlin et al., A new approach for analysis and evaluation of partial photoneutron reaction cross sections. Eur. Phys. J. A **50**, 114 (2014). https://doi.org/10.1140/epja/i2014-14114-x
18. V.V. Varlamov, A.I. Davydov, V.N. Orlin, Photonuclear partial reaction cross sections: Systematic uncertainties and reliability. At. Data Nucl. Data Tables **161**, 101697 (2025). https://doi.org/10.1016/j.adt.2024.101697
19. B.S. Ishkhanov, V.N. Orlin, N.N. Peskov et al., Photoneutron reactions in the range of giant dipole resonance. Phys. Part.

Nucl. **48**, 76–83 (2017). https://doi.org/10.1134/S1063779617010117
20. Y.L. Jin, Y. Tian, X. Tao et al., Theoretical calculation for photonuclear reactions of $^{142-146,148,150}$Nd. At. Energy Sci. Technol. **56**(5), 896–904 (2022). https://doi.org/10.7538/yzk.2022.youxian.0213
21. C. Cai, MEND-a code for calculating nuclear data of medium-heavy nuclei below 250 MeV. Nucl. Phys. Rev. **28**(3), 98–109 (2011). https://doi.org/10.11804/NuclPhysRev.28.03.354
22. P. Liu, H.Y. Zhang, X.F. Wu et al., Nuclear data processing and benchmarking for the test edition of China evaluated photonuclear data library (CENDL/PD-b). Ann. Nucl. Energy. **208**, 110745 (2024). https://doi.org/10.1016/j.anucene.2024.110745
23. T. Kawano, Y.S. Cho, P. Dimitriou et al., IAEA photonuclear data library 2019. Nucl. Data Sheets **163**, 109–162 (2020). https://doi.org/10.1016/j.nds.2019.12.002
24. TALYS-Based Evaluated Nuclear Data Library. https://tendl.web.psi.ch/tendl_2023/proton_html/proton.html
25. Japanese Evaluated Nuclear Data Library, Version 5. https://wwwndc.jaea.go.jp/jendl/j5/j5.html
26. G.A. Bartholomew, E.D. Earle, A.J. Ferguson et al., Gamma-ray strength functions. Adv. Nucl. Phys. **7**, 229–324 (1973). https://doi.org/10.1007/978-1-4615-9044-6_4
27. S. Goriely, P. Dimitriou, M. Wiedeking et al., Reference database for photon strength functions. Eur. Phys. J. A **55**, 172 (2019). https://doi.org/10.1140/epja/i2019-12840-1
28. V.V. Varlamov, B. Ishkhanov, V. Orlin, New data for the ^{197}Au (γ, nX) and ^{197}Au (γ, 2nX) reaction cross sections. Bull. Russ. Acad. Sci. Phys. **74**, 842–849 (2010). https://doi.org/10.3103/S1062873810060237
29. V.V. Varlamov, A. Davydov, B. Ishkhanov, Photoneutron cross sections for Co^{59}: systematic uncertainties of data from various experiments. Eur. Phys. J. A **53**, 180 (2017). https://doi.org/10.1140/epja/i2017-12373-7
30. A. Koning, S. Hilaire, S. Goriely, TALYS: modeling of nuclear reactions. Eur. Phys. J. A **59**, 131 (2023). https://doi.org/10.1140/epja/s10050-023-00935-7
31. V.V. Varlamovv, B. Ishkhanov, V. Orlin, Reliability of (γ, 1n), (γ, 2n), and (γ, 3n) cross-section data on Tb^{159}. Phys. Rev. C **95**, 054607 (2017). https://doi.org/10.1103/PhysRevC.95.054607
32. V.V. Varlamov, M. Makarov, N. Peskov, Photodisintegration of the isotopes Os^{186,188,189,190,192}: Similarities and distinctions. Phys. At. Nucl. **78**, 746–756 (2015). https://doi.org/10.1134/S1063778815060150
33. V.V. Varlamov, A. Davydov, B. Ishkhanov, The reliability of photoneutron cross sections for Zr^{90,91,92,94}. Eur. Phys. J. A **54**, 74 (2018). https://doi.org/10.1140/epja/i2018-12508-4
34. V.V. Varlamov, B.S. Ishkhanov, V.N. Orlin, Evaluated cross sections of photoneutron reactions on the isotope ^{116}Sn and spectra of neutrons originating from these reactions. Phys. At. Nucl. **80**, 1106–1118 (2017). https://doi.org/10.1134/S1063778817060230
35. V.V. Varlamov, V.N. Orlin, N.N. Peskov et al., Cross sections of partial photoneutron reactions for the ^{115}In nucleus and the neutron multiplicity sorting. Bull. Russ. Acad. Sci. Phys. **77**, 388–396 (2013). https://doi.org/10.3103/S1062873813040291
36. V.V. Varlamov, A.I. Davydov, V.N. Orlin, New evaluated data on ^{206,207,208}Pb photodisintegration. Eur. Phys. J. A **57**, 287 (2021). https://doi.org/10.1140/epja/s10050-021-00594-6
37. J. Kopecky, M. Uhl, Test of gamma-ray strength functions in nuclear reaction model calculations. Phys. Rev. C **41**(5), 1941–1955 (1990). https://doi.org/10.1103/PhysRevC.41.1941
38. D.M. Brink, Individual particle and collective aspects of the nuclear photoeffect. Nucl. Phys. **4**, 215–220 (1957). https://doi.org/10.1016/0029-5582(87)90021-6
39. P. Axel, Electric dipole ground-state transition width strength function and 7-MeV photon interactions. Phys. Rev. **126**, 671 (1962). https://doi.org/10.1103/PhysRev.126.671
40. S. Goriely, S. Hilaire, M. Girod et al., First Gogny-Hartree-Fock-Bogoliubov nuclear mass model. Phys. Rev. Lett. **102**(24), 242501 (2009). https://doi.org/10.1103/PhysRevLett.102.242501
41. S. Goriely, F. Tondeur, J.M. Pearson, A Hartree-Fock nuclear mass table. At. Data Nucl. Data Tables **77**(2), 311–381 (2001). https://doi.org/10.1006/adnd.2000.0857
42. S. Goriely, Radiative neutron captures by neutron-rich nuclei and the r-process nucleosynthesis. Phys. Lett. B **436**(1), 10–18 (1998). https://doi.org/10.1016/S0370-2693(98)00907-1
43. S. Goriely, E. Khan, M. Samyn, Microscopic HFB+QRPA predictions of dipole strength for astrophysics applications. Nucl. Phys. A **739**(3), 331–352 (2004). https://doi.org/10.1016/j.nuclphysa.2004.04.105
44. I. Daoutidis, S. Goriely, Large-scale continuum random-phase approximation predictions of dipole strength for astrophysical applications. Phys. Rev. C **86**(3), 034328 (2012). https://doi.org/10.1103/PhysRevC.86.034328
45. S. Goriely, S. Hilaire, S. Péru et al., Gogny-HFB+QRPA dipole strength function and its application to radiative nucleon capture cross section. Phys. Rev. C **98**(1), 014327 (2018). https://doi.org/10.1103/PhysRevC.98.014327
46. S. Goriely, V. Plujko, Simple empirical $E1$ and $M1$ strength functions for practical applications. Phys. Rev. C **99**(1), 014303 (2019). https://doi.org/10.1103/PhysRevC.99.014303
47. S. Goriely, N. Chamel, and J. M. Pearson, Hartree-Fock-Bogoliubov nuclear mass model with 0.50 MeV accuracy based on standard forms of Skyrme and pairing functionals. Phys. Rev. C **88**(6), 061302 (2013). DOI: https://doi.org/10.1103/PhysRevC.88.061302
48. A. Voinov, M. Guttormsen, E. Melby et al., γ-ray strength function and pygmy resonance in rare earth nuclei. Phys. Rev. C **63**(4), 044313 (2001). https://doi.org/10.1103/PhysRevC.63.044313
49. F.Q. Chen, Y.F. Niu, Y. Sun et al., Origin of the low-energy enhancement of the γ-ray strength function. Phys. Rev. Lett. **134**, 082502 (2025). https://doi.org/10.1103/PhysRevLett.134.082502
50. P. Fanto, Y. Alhassid, H.A. Weidenmüller, Statistical-model description of decay from compound-nucleus resonances. Phys. Rev. C **101**, 014607 (2020). https://doi.org/10.1103/PhysRevC.101.014607
51. R. Bergere, H. Beil, A. Veyssiere, Photoneutron cross sections of La, Tb. Ho and Ta. Nucl. Phys. A **121**, 463 (1968). https://doi.org/10.1016/0375-9474(68)90433-8
52. W. Luo, W. Xu, Q.Y. Pan et al., A 4D Monte Carlo laser-Compton scattering simulation code for the characterization of the future energy-tunable SLEGS. Nucl. Instrum. Meth. Phys. Res. Sect. A **660**(1), 108–115 (2011). https://doi.org/10.1016/j.nima.2011.09.035
53. W. Guo, W. Xu, J.G. Chen et al., A high intensity beam line of γ-rays up to 22 MeV energy based on Compton backscattering. Nucl. Instrum. Methods Phys. Res. A **578**(3), 457–462 (2007). https://doi.org/10.1016/j.nima.2007.05.322
54. H. Utsunomiya, I. Gheorghe, D.M. Filipescu et al., Direct neutron-multiplicity sorting with a flat-efficiency detector. Nucl. Instrum. Methods Phys. Res. A **871**, 135–141 (2017). https://doi.org/10.1016/j.nima.2017.08.001
55. Z.R. Hao, G.T. Fan, L.X. Liu et al., Design and simulation of 4π flat-efficiency ^{3}He neutron detector array. Nuclear Tech. (in Chinese) **43**(11), 110501 (2020). https://doi.org/10.11889/j.0253-3219.2020.hjs.43.110501

56. M.D. Zhou, Z.R. Hao, Q.K. Sun et al., Measurement of ^{59}Co(γ, n)^{58}Co using a new flat-efficiency neutron detector at the Shanghai Laser Electron Gamma Source. Phys. Rev. C **111**, 054612 (2025). https://doi.org/10.1103/PhysRevC.111.054612
57. L.X. Liu, H.W. Wang, G.T. Fan et al., The SLEGS beamline of SSRF. Nucl. Sci. Tech. **35**, 111 (2024). https://doi.org/10.1007/s41365-024-01469-3
58. Q.K. Sun, Y. Zhang, Z.R. Hao et al., Enhancing reliability in photonuclear cross-section fitting with Bayesian neural networks. Nucl. Sci. Tech. **36**, 52 (2025). https://doi.org/10.1007/s41365-024-01611-1
59. H.H. Xu, G.T. Fan, H.W. Wang et al., Interaction chamber for laser Compton slant-scattering in SLEGS beamline at Shanghai Light Source. Nucl. Instrum. Methods Phys. Res. A **1033**, 166742 (2022). https://doi.org/10.1016/j.nima.2022.166742
60. Z.C. Li, Y.X. Yang, W. Luo et al., Fast measurement of the quasi-monoenergetic MeV γ-beam flux using the ^{63}Cu(γ, n)^{62}Cu reaction at the Shanghai Laser Electron Gamma Source. Nucl. Instrum. Methods Phys. Res. B **559**, 165595 (2025). https://doi.org/10.1016/j.nimb.2024.165595
61. Q.K. Sun, Y. Zhang, Z.R. Hao et al., Study of photoneutron reaction based on physics-informed Bayesian neural network. Nuclear Tech. (in Chinese) **48**(5), 050001 (2025). https://doi.org/10.11889/j.0253-3219.2025.hjs.48.240501
62. W. Luo, Production of medical radioisotope ^{64}Cu by photoneutron reaction using ELI-NP γ-ray beam. Nucl. Sci. Tech. **27**, 96 (2016). https://doi.org/10.1007/s41365-016-0094-6
63. P.-A. Söderström, A. Kuşoğlu, D. Testov, Prospect for measurements of (γ, n) reaction cross-sections of p-nuclei at ELI-NP. Front. Astron. Space Sci. **10**, 1248834 (2023). https://doi.org/10.3389/fspas.2023.1248834